



**HAL**  
open science

## Controlled treatment of a high velocity anisotropic aquifer model contaminated by hexachlorocyclohexanes

Iheb Bouzid, Julien Maire, Fabien Laurent, Mathias Broquaire, Nicolas Fatin-Rouge

► **To cite this version:**

Iheb Bouzid, Julien Maire, Fabien Laurent, Mathias Broquaire, Nicolas Fatin-Rouge. Controlled treatment of a high velocity anisotropic aquifer model contaminated by hexachlorocyclohexanes. *Environmental Pollution*, 2021, 268, pp.115678. 10.1016/j.envpol.2020.115678 . hal-02962730

**HAL Id: hal-02962730**

**<https://hal.science/hal-02962730>**

Submitted on 17 Oct 2022

**HAL** is a multi-disciplinary open access archive for the deposit and dissemination of scientific research documents, whether they are published or not. The documents may come from teaching and research institutions in France or abroad, or from public or private research centers.

L'archive ouverte pluridisciplinaire **HAL**, est destinée au dépôt et à la diffusion de documents scientifiques de niveau recherche, publiés ou non, émanant des établissements d'enseignement et de recherche français ou étrangers, des laboratoires publics ou privés.



Distributed under a Creative Commons Attribution - NonCommercial 4.0 International License

# 1 Controlled treatment of a high velocity anisotropic aquifer model 2 contaminated by hexachlorocyclohexanes

3 Iheb Bouzid<sup>a</sup>, Julien Maire<sup>a</sup>, Fabien Laurent<sup>b</sup>, Mathias Broquaire<sup>c</sup>, Nicolas Fatin-Rouge<sup>a\*</sup>

4 <sup>a</sup> Université de Bourgogne Franche-Comté–Besançon, Institut UTINAM–UMR CNRS 6213, 16, route  
5 de Gray, 25030, Besançon, France

6 <sup>b</sup> SOLVAY, Centre de Recherche et Innovation de Lyon, DRP-ERA, 85 rue des Frères Perret 69192 Saint  
7 Fons

8 <sup>c</sup> SOLVAY, Direction Réhabilitation Environnement, Parc Everest, 54 rue Marcel Dassault 69740  
9 Genas

10 \* *Corresponding author, nicolas.fatin-rouge@univ-fcomte.fr*

11 Color is not required in print.

12

13 Abstract:

14 Xanthan gels were assessed to control the reductive dechlorination of hexachlorocyclohexanes  
15 (HCHs) and trichlorobenzenes (TCBs) in a strong permeability contrast and high velocity sedimentary  
16 aquifer. An alkaline degradation was selected because of the low cost of NaOH and Ca(OH)<sub>2</sub>. The  
17 rheology of alkaline xanthan gels and their ability to deliver alkalinity homogeneously, while  
18 maintaining the latter, were studied. Whereas the xanthan gels behaved like non-Newtonian shear-  
19 thinning fluids, alkalinity and Ca(OH)<sub>2</sub> microparticles had detrimental effects, yet, the latter  
20 decreased with the shear-rate. Breakthrough curves for the NaOH and Ca(OH)<sub>2</sub> in xanthan solutions,  
21 carried out in the lowest permeability soil (9.9 μm<sup>2</sup>), demonstrated the excellent transmission of  
22 alkalinity, while moderate pressure gradients were applied. Injection velocities ranging from 1.8 to  
23 3.8 m.h<sup>-1</sup> are anticipated in the field, given the permeability range from 9.9 to 848.7 μm<sup>2</sup>. Despite a  
24 permeability contrast of 8.7 in an anisotropic aquifer model, the NaOH and the Ca(OH)<sub>2</sub> both in

25 xanthan gels spread only 5- and 7-times faster in the higher permeability zone, demonstrating that  
26 the delivery was enhanced. Moreover, the alkaline gels which were injected into a high permeability  
27 layer under lateral water flow, showed a persistent blocking effect and longevity (timescale of  
28 weeks), in contrast to the alkaline solution in absence of xanthan. Kinetics of alkaline dechlorination  
29 carried out on the historically contaminated soil, using the  $\text{Ca}(\text{OH})_2$  suspension in xanthan solution,  
30 showed that HCHs were converted in TCBs by dehydrodechlorination, whereas the latter were then  
31 degraded by reductive hydrogenolysis. Degradation kinetics were achieved within 30 h for the major  
32 and most reactive fraction of HCHs.

33 **Capsule:** *In situ* remediation of a high velocity anisotropic aquifer historically contaminated by  
34 hexachlorocyclohexanes was assessed using alkaline reagents delivered in xanthan solutions

35

36 1. Introduction

37 Groundwater (GW) is an essential resource for drinking water production, because of its proximity  
38 and the purifying processes that occur during percolation [1,2]. In France, 96% of the catchments for  
39 drinking water industry are from GW, whereas this represents 66% of volumes [3]. Besides, GW also  
40 feeds natural ecosystems, whose health depends on its quality. GW quality has worsened, since  
41 anthropic pressure increased on that resource and because of contaminations from various origins.

42 In France, three-quarters of the soil and water pollution events involve organic compounds, among  
43 which chlorinated organic compounds (COCs) represent the majority [4]. Former industrial activities  
44 have engendered some major and persistent pollution issues. Lindane ( $\gamma$ -hexachlorocyclohexane)  
45 production and its use as a pesticide, was among the most impacting practices, because about  
46 450000 tons of this highly toxic and bioaccumulating molecule were used worldwide between 1950  
47 and 2000 [5–8]. This molecule and some of its seven hexachlorocyclohexane (HCH) isomers are part  
48 of the persistent organic pollutant list, because  $\alpha$ ,  $\beta$  and  $\delta$  isomers were co-produced by 70 to 90%  
49 [9–11]. Indeed, HCHs are unfortunately carcinogenic and detrimental to the nervous and to the  
50 endocrine systems [12]. Besides the background HCH-contamination, hot spots are found all over  
51 Europe, because of former production units or warehouses. Because of their toxicity, low water  
52 solubility and vapor pressure, HCHs remain in soils for decades [10]. There, they feed plumes of  
53 dissolved pollutants, causing the long-term quality degradation of water contacting them.

54 In E.U., the water framework directive 200/60/EC aims at the short-term recovery of good ecological  
55 status of natural water. The *in situ* remediation (ISR) of contaminated soils is growing, because it  
56 reduces the risks associated to contaminants dissemination and hazards [13]. Moreover, this strategy  
57 is especially advised when the access to contaminants is hindered, e.g. because of depth. Yet, ISR  
58 may be very technical in challenging situations, where underground heterogeneity and anisotropy  
59 hinder the access to contaminants. In particular, it is acknowledged that strong permeability  
60 contrasts hinder the homogeneous delivery of remediation fluids that mainly sweep through the

61 most permeable pathways [14–16]. Soil anisotropy leads to uncontrolled radii of influence (ROI),  
62 preferential flows and the heterogeneous distribution of amendments [17–23]. Thus, low  
63 permeability zones where contaminants are often trapped are badly swept and remain untreated.  
64 Besides the rise of costs for remediation, several effects like back diffusion tailing and rebound are  
65 often observed, which hinder the lasting recovery of GW quality due to ineffective treatments [24].

66 Fighting the fingering of injected fluids requires to increase their capillary number [25,26]. This well-  
67 known trouble led to the use of viscous, but shear-thinning fluids in oil recovery [14,27–30]. These  
68 behaviors, observed for associative polymers like xanthan and for foams, are used for the ISR of  
69 contaminated soils [20,21,23,31–42].

70 Fortunately, several means exist to remove HCH, among which chemical degradation is especially  
71 suitable for low to medium range contaminant concentrations [12,43–45]. *In situ* dechlorination *via*  
72 chemical reduction is often suitable for the degradation of COCs in the underground, because of the  
73 low concentrations of oxidizing molecules. Despite the fact that many studies have highlighted the  
74 interest of nano-zero-valent iron (nZVI), obvious barriers raised, such as cost, persistence, and health  
75 concerns [46–48]. Besides, alkaline degradation of HCHs could be a cheaper alternative [10,48,49]. It  
76 might be beneficial for the environment because of the lower toxicity of degradation products  
77 [44,49]. Yet, one should use carefully alkaline reagents like quicklime, since they may engender  
78 hazardous reactions and metabolites [50,51]. Half-lives for the alkaline degradation (pH=11.7) of  
79 most HCHs dissolved in ethanol/water mixtures are reported to range from 0.5 to 1h at 20°C [52].  
80 However, hydrophobic HCHs desorb slowly from soils and require persistent action, especially in high  
81 velocity aquifers [24]. There, an aqueous Ca(OH)<sub>2</sub> suspension could be a long-lasting reagent to  
82 maintain alkalinity, considering its delayed dissolution.

83 This paper reports a laboratory study about a high velocity and strongly heterogenous aquifer  
84 contaminated by HCHs and trichlorobenzenes (TCBs). In that challenging situation, the control of  
85 amendment delivery and the continued blocking of GW flow in the treated zone are critical for the

86 achievement of the remediation. Therefore, the study aims at assessing the performances of xanthan  
87 solutions to deliver persistent alkali in strong permeability-contrasted aquifers and maintaining their  
88 action. It also provides accurate information on kinetics of COCs degradation involved in the  
89 remediation of the contaminated aquifer.

90

## 91 2. Materials and methods

### 92 2.1 Contaminated soils

93 The studied soil was collected using non-destructive sonic core sampling at a former lindane  
94 production facility. Site characterization shown the contaminated aquifer was strongly  
95 heterogeneous, with no geological continuity, and cm to m-scale variations. In addition, no  
96 correlation was evidenced between contamination and soil permeability. Spatial size distribution of  
97 soil particles was characterized by sieving [53]. Three model soil fractions (fine sand, medium sand  
98 and coarse sand) having  $D_{10}$ - $D_{90}$  of 54-600, 160-600 and 80-2100  $\mu\text{m}$ , respectively, were obtained  
99 through sieving.  $D_{10}$  and  $D_{90}$  correspond to the 10<sup>th</sup> and 90<sup>th</sup> percentile of grain size distribution,  
100 respectively. Permeabilities ( $k$ ) of the model soils were 9.9, 96.7 and 848.7  $\mu\text{m}^2$ , respectively, as  
101 measured using the constant head technique [54]. These permeabilities were mainly chosen to  
102 recreate permeability contrasts in sandboxes closer to those measured from soil cores. The  
103 porosities of the materials were 0.32 for the fine and medium sands and 0.34 for the coarse one.  
104 Porosity was measured by weighing a column before and after filling it with water to determine the  
105 porous volume (PV) of the soil sample [55]. Given the complex contamination generated by lindane  
106 production, the fine sand (9.9  $\mu\text{m}^2$ ) was characterized by the concentrations of the detected  
107 contaminants, namely  $\alpha$ ,  $\beta$ ,  $\gamma$  and  $\delta$ -HCH isomers, and 1,2,3 and 1,2,4-TCB isomers. The contaminated  
108 soils were collected in sealed flasks and stored upside-down to avoid contaminants volatilization.

### 109 2.2 Chemicals

110 Xanthan gum (Rhodicare) was supplied by SOLVAY in the form of a dry powder. Xanthan solutions  
111 were prepared by dispersing the required amount of solid polymer in deionized water. The  
112 suspensions were heated (70°C) under stirring for 45 min. until the solubilization of the polymer and  
113 the achievement of a clear solution. Sodium hydroxide (> 97%, Fisher) and calcium chloride (98%,  
114 Prolabo) were used to prepare aqueous  $\text{Ca}(\text{OH})_2$ : NaOH and  $\text{CaCl}_2$  were directly solubilized in two  
115 0.2% xanthan solutions to a concentration of 0.6% corresponding to a  $\text{Ca}(\text{OH})_2$  concentration of 0.3%

116 after mixing the two solutions. Finally, the resulting  $\text{Ca}(\text{OH})_2$  suspension in xanthan solution was  
117 dispersed using a high-performance dispersing instrument at 25000 rpm for 3 min. (ultra-turrex®, IKA  
118 T25). The obtained fluid was not filtered before injection. The  $\text{Ca}(\text{OH})_2$  microparticles obtained were  
119 characterized by optical microscopy (Nachet 300) and had an average size of  $8\pm 2 \mu\text{m}$ . Eosin (Acros  
120 Organics) was used to color the circulating water in the sandbox, mimicking the natural GW flow.  
121 Phenolphthalein and sulfuric acid (Fisher) were used for the acid-base determination of alkalinity.  
122 The universal indicator (Fisher) was chosen to monitor pH changes of the injected alkaline fluids in  
123 sandbox. Acetone (>99%, Fisher) and n-hexane (95%, Fisher) were used as solvents to extract the  
124 contaminants from soils. 1,2,4-TCB (99%), 1,2,3-TCB (99%), 1,3,5-TCB (98%), 1,2-dichlorobenzene  
125 (DCB, 98%), 1,3-DCB (98%), 1,4-DCB (>99%), chlorobenzene (CB, 99%) were obtained from Alfa Aesar.  
126 A solution containing a mixture of HCH isomers (Fisher) and benzene (99%, Janssen Chemica) was  
127 used for the standards preparation in methanol (>99%, Fisher).

### 128 2.3 Bulk viscosity measurements

129 Bulk rheological characterization of the xanthan solutions was performed using a rotational  
130 rheometer (Malvern Kinexus pro+) equipped with a cone-plate measuring system. Rheological  
131 measurements were carried out at 25°C. Eighty measurement points were repeated 4-times for each  
132 solution.

### 133 2.4. Alkalinity transport and experimental set-up

134 The rheological behavior of injected alkaline (NaOH 0.1% M and  $\text{Ca}(\text{OH})_2$  at 0.3%) xanthan-based  
135 fluids through porous medium were performed in columns (l: 0.1 to 0.4 m, i.d.: 3.2 cm, PV = 56 mL)  
136 and in sandboxes (dim.: 2×18×25 cm, PV = 276 mL). The experimental set-up is illustrated in Figure 1.  
137 The soils were packed wet and gently vibrated to ensure a uniform packing.  
138 The fine and coarse materials ( $k = 9.9$  and  $848.7 \mu\text{m}^2$ ) were used in the columns experiments. The  
139 sandbox was filled under water with medium and coarse sands ( $k = 96.7$  and  $848.7 \mu\text{m}^2$ ) to make a  
140 representative elementary volume (REV) and an average permeability contrast of 8.7, as deduced



141 from the site characterization. The soil was held at the top of the sandbox by a rigid plate. The water  
142 circulation simulating the GW flow was injected with a peristaltic pump (Masterflex) connected to a  
143 water tank and to a perforated tube (HDPE, d.: 2 cm) placed on the left side of the sandbox. The  
144 average water circulation rate was 10 m.d<sup>-1</sup>. The recovery of water flowing through the sandbox was  
145 performed using a second perforated tube at the right end. The water recovered from this second  
146 well was collected into another glass flask. The reagent solutions were injected through an opening  
147 at the back center of the sandbox (Fig. 1).

148 The reagent solutions were maintained under mechanical agitation (600 rpm) and they were injected  
149 using a dosing pump (KNF Simdos 10). The pressures were recorded automatically with an automate  
150 (Arduino Uno) connected to a computer.

151 The apparent viscosities of the injected solutions were measured in columns from pressure drops at  
152 Darcy flow rates of 1.98×10<sup>-4</sup>, 3.96×10<sup>-4</sup>, 6.60×10<sup>-4</sup> and 10.6×10<sup>-4</sup> m.s<sup>-1</sup>.

153 The alkalinity breakthrough curves were carried out in columns (l: 0.1 to 0.4 m, i.d.: 3.2 cm) filled  
154 with fine sand (9.9 μm<sup>2</sup>). The alkaline xanthan solutions were injected at a rate of 6.60×10<sup>-4</sup> m.s<sup>-1</sup>.  
155 The alkalinity of the recovered effluent was monitored by sulfuric acid titration. The reference value  
156 was the alkalinity of the fluids before injection. A total of 9 PVs were injected. Breakthrough curves  
157 were obtained by plotting the ratio of the alkaline concentration  $C$  measured in the effluent at time  $t$   
158 and the one of the injected fluid  $C_0$ , vs. time. The estimation of the Darcy velocity  $u$ (m.s<sup>-1</sup>) and of the  
159 tracers dispersivity  $\alpha$ (m) is possible using the solution of the advection-dispersion equation in semi-  
160 infinite column [56]:

$$161 \frac{C}{C_0} = 0.5 \cdot \left[ \operatorname{erfc} \left( \frac{x-u \cdot t}{\sqrt{4 \cdot \alpha \cdot u \cdot t}} \right) + \exp \left( \frac{x \cdot u}{D} \right) \cdot \operatorname{erfc} \left( \frac{x+u \cdot t}{\sqrt{4 \cdot \alpha \cdot u \cdot t}} \right) \right] \quad (1)$$

162 where  $x$ (m) is the length of the column and  $D$ (m<sup>2</sup>.s<sup>-1</sup>) is the dispersion coefficient.

163 When  $x/\alpha$  is large, the second term can be neglected and the eq. 1 becomes:

164  $\frac{c}{c_0} \sim 0.5 \cdot \operatorname{erfc}\left(\frac{x-ut}{\sqrt{4\alpha ut}}\right)$  (1')

165 Values of  $u$  and  $\alpha$  were fitted from the breakthrough curve for the NaOH in xanthan solution  
166 assuming that it was a small conservative tracer. Then setting the obtained  $\alpha$ -value, the retardation  
167 factor for the  $\text{Ca}(\text{OH})_2$  suspension in xanthan solution was calculated as the ratio of the Darcy  
168 velocities fitted from the NaOH and the  $\text{Ca}(\text{OH})_2$  breakthrough curves, respectively. Besides,  
169 considering some irreversible trappings of  $\text{Ca}(\text{OH})_2$  particles, a transmission factor was calculated  
170 from the plateaus-value of the  $C/C_0$  ratio at long times, assuming a steady-state regime.

171 At the end of the transport experiments, the column was sacrificed for the evaluation of spatial  
172 distribution of alkalinity. The column was dissected into 20 segments of 2 cm and the soil alkalinity  
173 was measured in each section to better assess the  $\text{Ca}(\text{OH})_2$  transport. The collected soil fractions  
174 were placed in a beaker containing 20 mL of pure water. Then, some drops of phenolphthalein were  
175 added, before the alkalinity was titrated under agitation with sulfuric acid.

176 The alkaline xanthan-based fluids injected into the sandbox were colored by the universal pH  
177 indicator (purple color at pH 12). The universal indicator (0.05%w) allowed the visualization of the  
178 solutions propagation and the observation of possible pH changes in the treated area over time. The  
179 injection of alkaline solutions in the most permeable layer was stopped when the edges of the  
180 sandbox were reached.

181

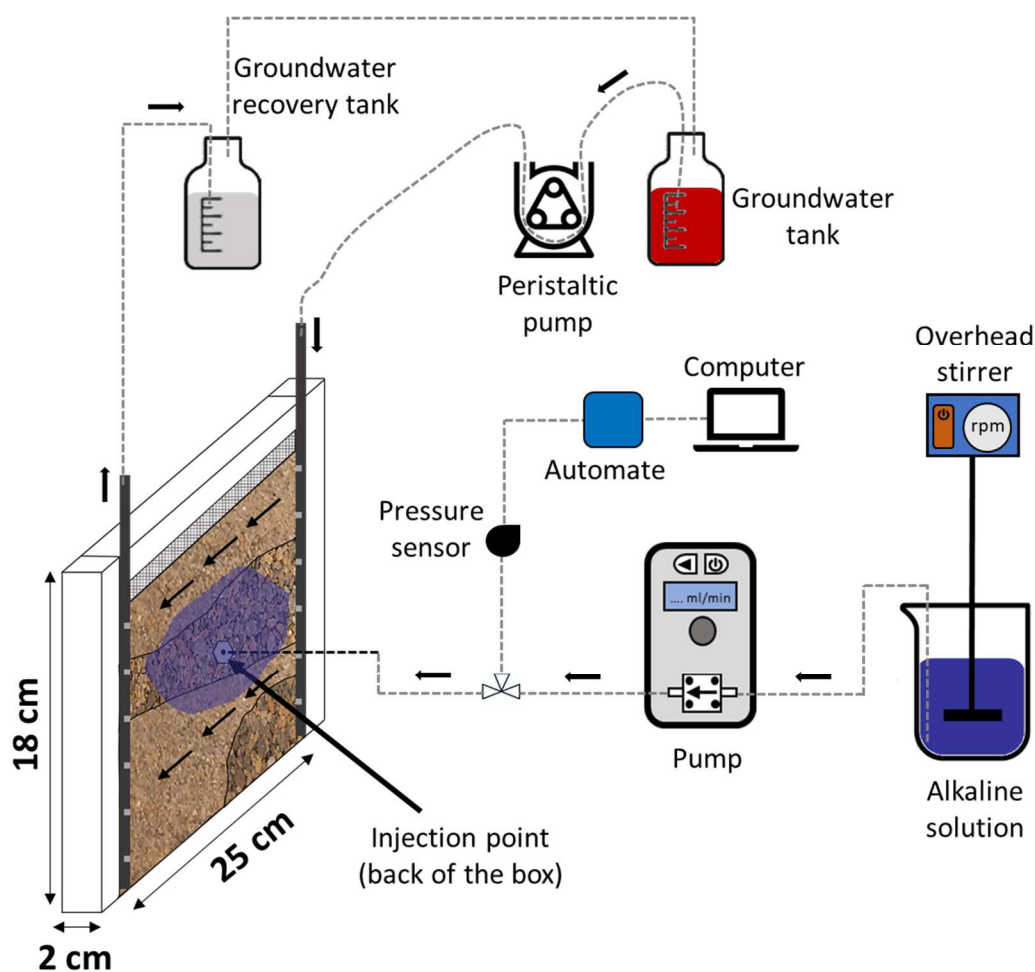


Figure 1. Experimental set-up used for the injections of solutions.

## 182 2.5 Kinetics of contaminants degradation

183 The kinetic study of HCH and TCB degradation was carried out in short columns (l: 5 cm, i.d.: 3.2 cm).  
 184 Each column was prepared with approximately 60 g of fine sand from the contaminated site. For  
 185 each column, 1 PV of xanthan solution (0.2%) carrying  $\text{Ca}(\text{OH})_2$  (0.3%, pH 12) was injected. The  
 186 reaction was monitored at 20°C for 72h. Columns were sacrificed at different times for the analysis of  
 187 HCH and TCB concentrations. The untreated soil was used as a reference for initial contaminant  
 188 concentrations. The experiments were duplicated, and the averaged results were used.

189 The kinetics of HCH disappearance was pseudo first-order. The kinetic constants ( $\text{h}^{-1}$ ) for HCH were  
 190 obtained by non-linear fitting of concentrations vs. time. TCBs kinetic constants were obtained by  
 191 fitting their concentrations using eq. 2:

192 
$$C = \frac{k_1 C_0}{k_2 - k_1} (e^{-k_1 t} - e^{-k_2 t}) \quad (2)$$

193 where  $C_0$  is the initial TCB concentration,  $k_1$  and  $k_2$  ( $\text{h}^{-1}$ ) are the average rate constants for HCH and  
194 TCB degradation, respectively.

## 195 2.6 Analytical methods

196 Contaminants were extracted from the solid matrix using a Soxhlet. The soils from each column and  
197 the reference material were extensively washed by recycling 80 mL of a hexane/acetone mixture  
198 (1/1w), for 4 h, in a heated reflux (80°C). The recovered organic phase was reported to 100 mL and  
199 diluted if necessary. It was then dehydrated with anhydrous sodium sulphate before analysis. HCH  
200 and TCB were analyzed by GC-MS (Perkin Elmer in liquid mode, Restek Rxi-5SilMS 30 m capillary  
201 column with 0.25 mm i.d., film thickness 0.25  $\mu\text{m}$ ) according to NF EN ISO 6468 and NF EN ISO 10301  
202 standards, respectively. For volatile compounds (DCB, CB and benzene), the analysis was carried out  
203 directly on the solid sample by GC-MS in static headspace (Thermo Trace DSQ with PTV injector), by  
204 adapting the NF EN ISO 10301 standard. The vial was incubated at 70° for 30 min. Then, 1 mL of the  
205 vapor phase was collected (syringe temperature: 77°) and directly injected. Helium was used as a  
206 carrier gas with a constant flow rate of 1  $\text{mL}\cdot\text{min}^{-1}$ . The quantification limit (QL) of individual  
207 compounds (in parentheses) was 4.2  $\mu\text{g}\cdot\text{kg}^{-1}$  (HCH), 33.3  $\mu\text{g}\cdot\text{kg}^{-1}$  (TCB) and 0.01 (1,3-DCB), 0.013 (1,2-  
208 DCB), 0.014 (1,4-DCB), 0.01  $\text{mg}\cdot\text{kg}^{-1}$  (CB), respectively. All compounds were identified using analytical  
209 standards prepared in methanol. Phenol index was measured by adapting ISO 6439 standard by UV-  
210 Vis spectrophotometry (Perkin Elmer Lambda 45) at 510 nm. The QL for the phenol index was 0.5  
211  $\text{mg}\cdot\text{kg}^{-1}$ .

## 212 3. Theory

213 The overall rheological behavior of xanthan solutions can be described using the Cross model [57]:

214 
$$\eta = \frac{\eta_0 - \eta_\infty}{(1 + \lambda \dot{\gamma})^m} + \eta_\infty \quad (3)$$

215 where  $\eta_0$  and  $\eta_\infty$  are the asymptotic values of viscosity at low and very high shear rates,  $\dot{\gamma}$  is the  
216 effective shear rate within the porous medium,  $m$  measures the degree of dependence of viscosity  
217 on the shear rate in the shear-thinning region, while  $\lambda$  is related to the shear rate value where shear-  
218 thinning behavior starts ( $s^{-1}$ ).

219 The apparent viscosity of the injected solutions in columns  $\eta_{app}$  is defined on the basis of Darcy law:

$$220 \quad \eta_{app} = \frac{k}{u} \frac{\Delta P}{l} \quad (4)$$

221 where  $k$  is the permeability ( $m^2$ ),  $u$  is the Darcy flow rate ( $m \cdot s^{-1}$ ),  $\Delta P$  is the pressure drop (Pa) over a  
222 length  $l$  (m) of a porous medium.

223 The effective shear-rate within the porous medium ( $\dot{\gamma}_{mp}$ ) is defined according to [58]:

$$224 \quad \dot{\gamma}_{mp} = \frac{\beta \cdot u}{\sqrt{k \cdot \varepsilon}} \quad (5)$$

225 where  $\beta$  is a shift factor between the porous medium and bulk and is a function of both the bulk  
226 rheology and the porous structure, and  $\varepsilon$  is the effective porosity of the medium.

## 227 4. Results and discussion

### 228 4.1 Rheology of xanthan solutions and distribution of alkalinity

#### 229 4.1.1 Bulk and column measurements

230 The viscosity of xanthan solutions as a function of the shear-rate are shown in Fig. 2a. An alkalinity-  
231 free xanthan solution was used as a reference. Alkalinity has detrimental effects on both viscosity  
232 and shear-thinning behavior of the xanthan solutions [59]. This results from the perturbation of the  
233 associative behavior of xanthan, which can be attributed to either polymer hydrolysis or lower  
234 interpolymer H-bonds density in alkaline medium. Obviously, this perturbation increases in presence  
235 of  $Ca(OH)_2$  microparticles, nevertheless, the fluid viscosity remains 400-times higher than for pure  
236 water.

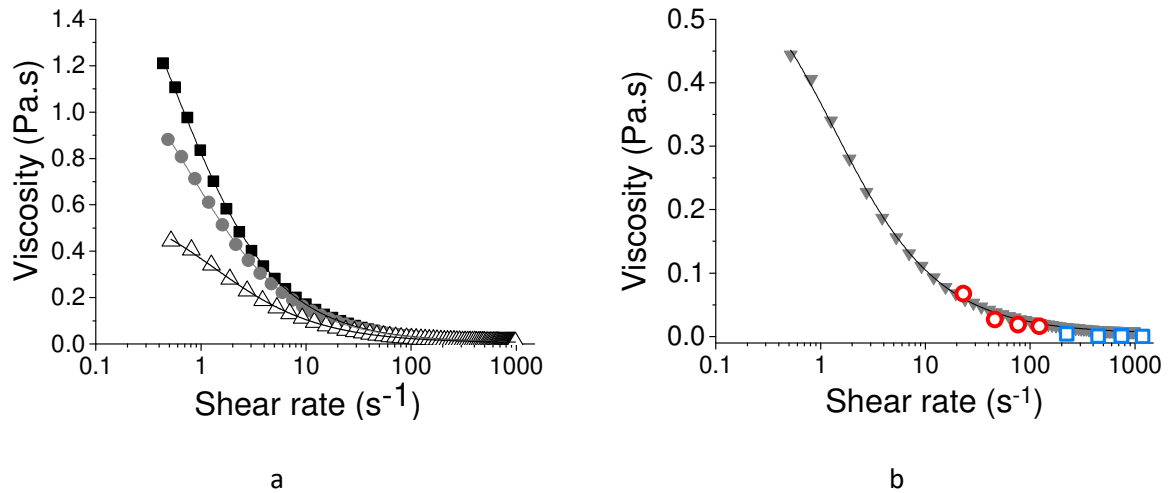


Figure 2. a) Bulk rheology of xanthan (0.2%w) solutions : Xanthan (■), NaOH in xanthan solution (●), Ca(OH)<sub>2</sub> suspensions in xanthan solution (Δ). Lines show fits of experimental data using eq. 3. b) Bulk and porous medium rheologies of the Ca(OH)<sub>2</sub> suspensions in xanthan solution (0.3%/0.2%w). Data from bulk (▼) and soil materials (○:  $k= 9.9 \mu\text{m}^2$  and □:  $k= 848.7 \mu\text{m}^2$ ). Pure water viscosity :  $8.90 \times 10^{-4} \text{ Pa}\cdot\text{s}$ .

237 The Cross parameters extracted from experimental data, using eq. 3, are presented in Table SM1.

238 The parameters reveal the strong detrimental effect of alkaline amendment on the fluid viscosity at

239 low shear-rates; decreases amounted to 33 and 70% for the NaOH solution and the Ca(OH)<sub>2</sub>

240 suspension in xanthan solution, respectively. However, and most important for injection in soils, the

241 detrimental effect of amendment on viscosity is much lower at high shear-rates. Besides, the shear-

242 thinning behavior starts at lower shear-rates in presence of alkalinity, which is explained by its

243 detrimental effect on polymer association.

244 The porous medium rheogram obtained from the injections of the Ca(OH)<sub>2</sub> suspension in xanthan

245 solution in soils are shown with the bulk rheogram in Fig. 2b. Those results were obtained using

246 equations 4 and 5 from the pressure gradients measured during the single-step injections in soil-

247 columns (Fig. SM1). A shift factor  $\beta$  of two was used to get the overlap between the two curves. This

248 factor depends on the structure of the porous material, especially on the tortuosity. Values close to

249 the unit were reported for simple materials like uniform glass beads [40,41,60]. However, higher

250 values (1.7-2.4) were obtained for the injection of amendments, like nZVI, suspended in xanthan  
251 solution in sands [61,62]. Nevertheless, shift factors close to one show that the bulk rheological  
252 characterization allows the good estimation of pressure gradients in the porous medium [40]. In this  
253 study, the rheologies of the  $\text{Ca}(\text{OH})_2$  suspension in xanthan solution in bulk and in the soils were  
254 similar. This demonstrates that the shear-thinning behavior increases with the shear-rate in these  
255 soils. The lower the soil permeability, the higher the shear-rate is, and the lower the fluid viscosity is.  
256 For injections in soils, shear-rates were ranging between 20 and  $2000 \text{ s}^{-1}$  (Fig. 2b) and, as explained  
257 above, the detrimental effect of amendment on fluid viscosity is lower at these high rates. Hence,  
258 injections should be performed at the highest velocity, being careful to avoid soil fracturing by not  
259 exceeding a pressure gradient larger than  $0.1 \text{ MPa}\cdot\text{m}^{-1}$  [63]. The  $\text{Ca}(\text{OH})_2$  suspension in xanthan  
260 solution can be easily injected because of the moderate pressure gradients recorded. In coarse sand,  
261 the injection velocity should be at least  $3.8 \text{ m}\cdot\text{h}^{-1}$ , considering that the recorded pressure gradient  
262 was only  $0.03 \text{ MPa}\cdot\text{m}^{-1}$ . However, the injection velocity should be about  $1.8 \text{ m}\cdot\text{h}^{-1}$  in fine sand. Those  
263 velocities are common for injections of amendments in the underground [64].

264 The alkalinity breakthrough curves in fine sand ( $k=9.9 \mu\text{m}^2$ ) for NaOH and for  $\text{Ca}(\text{OH})_2$  suspension  
265 (0.3%, d.:  $8\pm 2 \mu\text{m}$ ) in xanthan solution are shown in Fig. 3a. The plateaus for the relative alkalinity at  
266 the output of the column reached the unit after less than 9 PV injected. Obviously, the plateau was  
267 reached more rapidly for NaOH, which travelled like a conservative tracer. Fitted values for NaOH  
268 using eq. 1' were  $(7.1\pm 0.9)\times 10^{-3} \text{ m}$  for dispersivity and  $(6.44\pm 0.05)\times 10^{-3} \text{ m}\cdot\text{s}^{-1}$  for its Darcy-velocity.  
269 For  $\text{Ca}(\text{OH})_2$ , experimental data were analyzed assuming a one-component alkalinity, considering the  
270 simplicity of the model and the chi-squared values, and a trapping factor, since the plateaus value of  
271  $C/C_0$  was less than one. The average Darcy velocity for the alkalinity was  $(5.11\pm 0.19)\times 10^{-3} \text{ m}\cdot\text{s}^{-1}$ ,  
272 leading to a retardation factor of 1.2 compared with NaOH. Besides, a transmission factor of 91% was  
273 calculated for the alkalinity. This demonstrates a fast and high transmission of the alkalinity for the  
274  $\text{Ca}(\text{OH})_2$  suspension through this low permeability medium, despite about half was in the solid form  
275 as calculated from the solubility product ( $4.7\times 10^{-6}$  at  $25^\circ\text{C}$ ). This is explained by the fast equilibrium

276 between the dissolved and the solid forms of  $\text{Ca}(\text{OH})_2$ . Yet, a slower release of alkalinity in GW is  
277 expected after the injection of the  $\text{Ca}(\text{OH})_2$  suspension in the treated zone.

278 Similar results were reported for the transport of nano and micro ZVI by xanthan solutions using  
279 comparable injection velocities [33,40,41,65]. Tiraferri and Sethi [66] have reported the effect of guar  
280 gum on the polyaspartate-stabilized nZVI injectability in fine sand. The comparison of the  
281 breakthrough curves showed a 3-times improvement for the iron transport in presence of guar gum.  
282 However, nZVI accumulated faster at high injection rates, while initial concentrations at the output  
283 were higher. The same observation was reported in presence of polyvinylpyrrolidone in columns filled  
284 with glass beads [67]. The relative concentration of the transmitted amendment increased by 18-  
285 times and was reached 4-times faster. Hence, viscous polymer solutions limit particles aggregation.  
286 They also enhance the treatment efficiency in soils, as expected from the increased viscous pressure  
287 of xanthan solutions.

288 After the  $\text{Ca}(\text{OH})_2$  transport experiments were performed, the soil columns were sacrificed and the  
289 alkalinity was measured in each 2 cm-portions from the input (Fig. 3b). Alkalinity accumulation was  
290 observed at the column input. It decreased exponentially with the distance to reach coarsely the  
291 value of the injected suspension. This exponential behavior is explained by the balance equation on  
292 amendment injection through a filter medium. However, in that case, the observed accumulation  
293 only resulted from the delayed transmission of alkalinity, due to the size of the  $\text{Ca}(\text{OH})_2$   
294 microparticles. Experimental data were fitted using the following eq. :

$$295 \quad C/C_0 = A + B e^{(-\kappa x)} \quad (6)$$

296 where  $A = 1.09 \pm 0.072$ ,  $B = 7.80 \pm 0.366$  and  $\kappa = 0.176 \pm 0.0125 \text{ cm}^{-1}$  ( $R^2 = 0.98$ ).

297 The A-value matches perfectly with the transmission factor calculated from the breakthrough curve.  
298 Besides, a  $\kappa$ -value of  $0.612 \text{ cm}^{-1}$  was reported for the transport of nZVI in  $4.93 \times 10^{-11} \text{ m}^2$  sand  
299 columns [68]. Also, values of  $0.364$  et  $0.260 \text{ cm}^{-1}$  were reported for the transmission of nZVI using



300 pure water and viscous foam, respectively [69], demonstrating that the transport of particles is  
 301 enhanced for fluids with higher capillary number as expected from fluids with higher viscous force.  
 302 Despite the size of  $\text{Ca}(\text{OH})_2$  microparticles, the  $\kappa$ -values reported in literature were 2 to 4-times  
 303 larger. The lower retention observed in the present study is explained by the higher viscosity of the  
 304 xanthan solution (higher fluid capillary number) and because half of the  $\text{Ca}(\text{OH})_2$  was dissolved.  
 305 Similar observations were reported for the transport of iron particles by xanthan solutions  
 306 [33,60,65]. For the transport of nZVI in glass beads columns and in presence of xanthan (0.3%), the  
 307 relative iron concentration decreased from 5 to one over a 0.3 m distance [60]. In contrast, the  
 308 transmission of Ag nanoparticles through sand was very bad when the latter were suspended in pure  
 309 water [70].

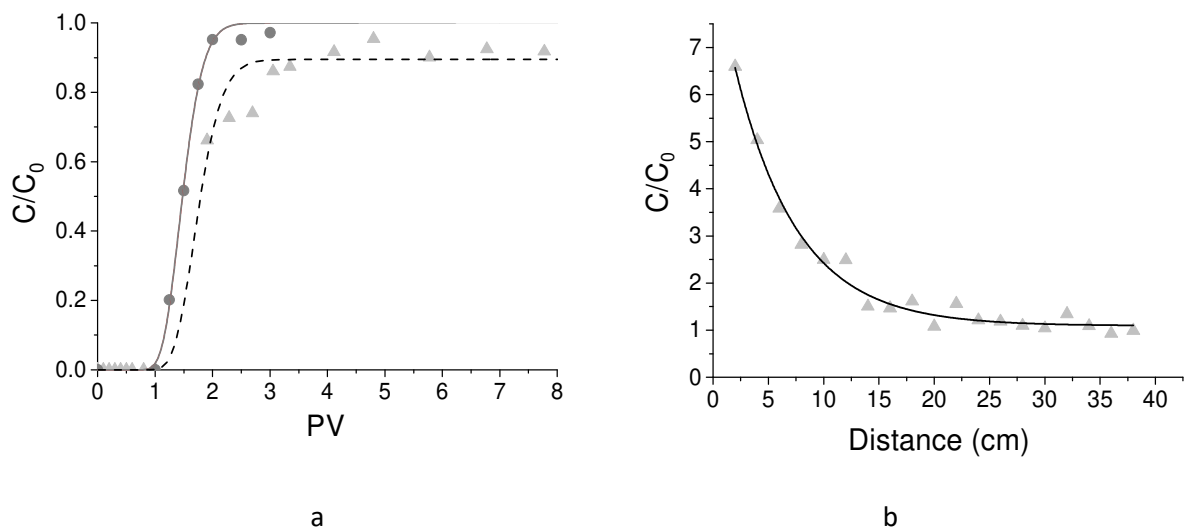


Figure 3. a) Breakthrough curves of alkalinity for NaOH (●, 0.027 M, solid line) and  $\text{Ca}(\text{OH})_2$  (▲, 0.3%, dashed line) in xanthan solution (0.2%) in the low permeability ( $9.9 \mu\text{m}^2$ ) contaminated soil column (L: 0.4 m, i.d. 3.5 cm). b) Alkalinity variations along the soil column after transmission measurements for the  $\text{Ca}(\text{OH})_2$  suspension in xanthan solution.

310

311 4.1.2 Measurements in permeability-contrasted sandbox

312 Regarding the random and cm-scale variations of the contaminated heterogeneous aquifer, it is  
313 impossible to control in which soil permeability the treatment fluid is injected. Therefore, it was  
314 decided to study the worst scenario, corresponding to the injection of the treatment fluid in the most  
315 permeable material, to see how far the treatment fluid could spread isotropically in the surrounding  
316 materials and resist to GW flow. The enhanced distribution and the persistence of alkalinity (pH 12,  
317 purple colored) in anisotropic porous medium, under lateral GW flow, using 0.2% xanthan solutions,  
318 were studied. The water circulation was used to simulate the GW flow through this REV. A NaOH  
319 solution in pure water was used as a reference fluid to compare the behaviors of the dissolved NaOH  
320 and the  $\text{Ca}(\text{OH})_2$  suspension in xanthan solutions. A longer-lasting alkalinity was expected for the  
321  $\text{Ca}(\text{OH})_2$  suspension, because half the alkalinity was in the solid state and its delayed concentration-  
322 controlled dissolution. All these alkaline fluids were injected at the back center of the sandbox in a  
323 high permeability material (HPM), as shown in Fig. 4. Despite the fact that each fluid mainly  
324 propagated in the HPZ, the xanthan-based ones also entered into the surrounding low permeability  
325 material (LPM), as previously observed [32,62,71]. Yet, in agreement with its higher shear-thinning  
326 behavior, the NaOH in xanthan solution better penetrated the LPM than the  $\text{Ca}(\text{OH})_2$  suspension in  
327 xanthan solution. Indeed, alkalinity propagated 5- and 7-times faster in the HPM than in the LPM for  
328 the NaOH in xanthan solution and the  $\text{Ca}(\text{OH})_2$  suspension in xanthan solution, respectively. Besides,  
329 in contrast to the alkaline water solution, no fingering was observed during the injection of the  
330 viscous xanthan-based fluids, which means a better controlled delivery. Hence, as expected, the  
331 increased capillary number of the injected fluids and their shear-thinning behavior allowed to control  
332 better viscous fingering and the sweeping of this anisotropic medium.

333 As shown in Fig. 4, once the injection of alkaline fluids was achieved, the simulated GW flow was  
334 colored (red), to study their longevity into the treated zone. In absence of xanthan, only 0.68 PV of  
335 GW removed all the injected alkalinity. The resulting solution became blue, corresponding to a pH  
336 increase between 10 and 11, because of the fast leaching of alkalinity by the GW flow. In contrast,  
337 the GW flow was effectively diverted in the LPM, when xanthan solutions were injected in the HPM.

338 The effectiveness of flow diversion was revealed as a clear inversion of permeability occurred, since  
 339 the treated layer became 2.6- and 2.9-times less permeable than the LPM for the  $\text{Ca}(\text{OH})_2$  in xanthan  
 340 and the NaOH in xanthan fluids, respectively. Hence, the injection of the xanthan solutions produced  
 341 a markedly long-lasting blocking effect, which diverted GW flow out of the treated zone. This effect  
 342 was also observed for the monitored pH-values at the output of the cell, which displayed a striking  
 343 difference associated to the presence of xanthan (Fig. SM3). Whereas a sharp wave of alkalinity with  
 344 pH up to 10.4 was observed in absence of xanthan, no significant pH change occurred in its presence.  
 345 The strong mobility difference between GW and the xanthan solution is associated to the viscous and  
 346 shear-thinning behaviors of the latter. It engenders persistent blocking and GW diverting flow that  
 347 ensure the long-lasting activity of the alkaline reagent into the treated zone. A similar blocking  
 348 behavior was reported using poly N-isopropylacrylamide, which was attributed to polymer  
 349 aggregation blocking the water flow at pores constrictions [72].

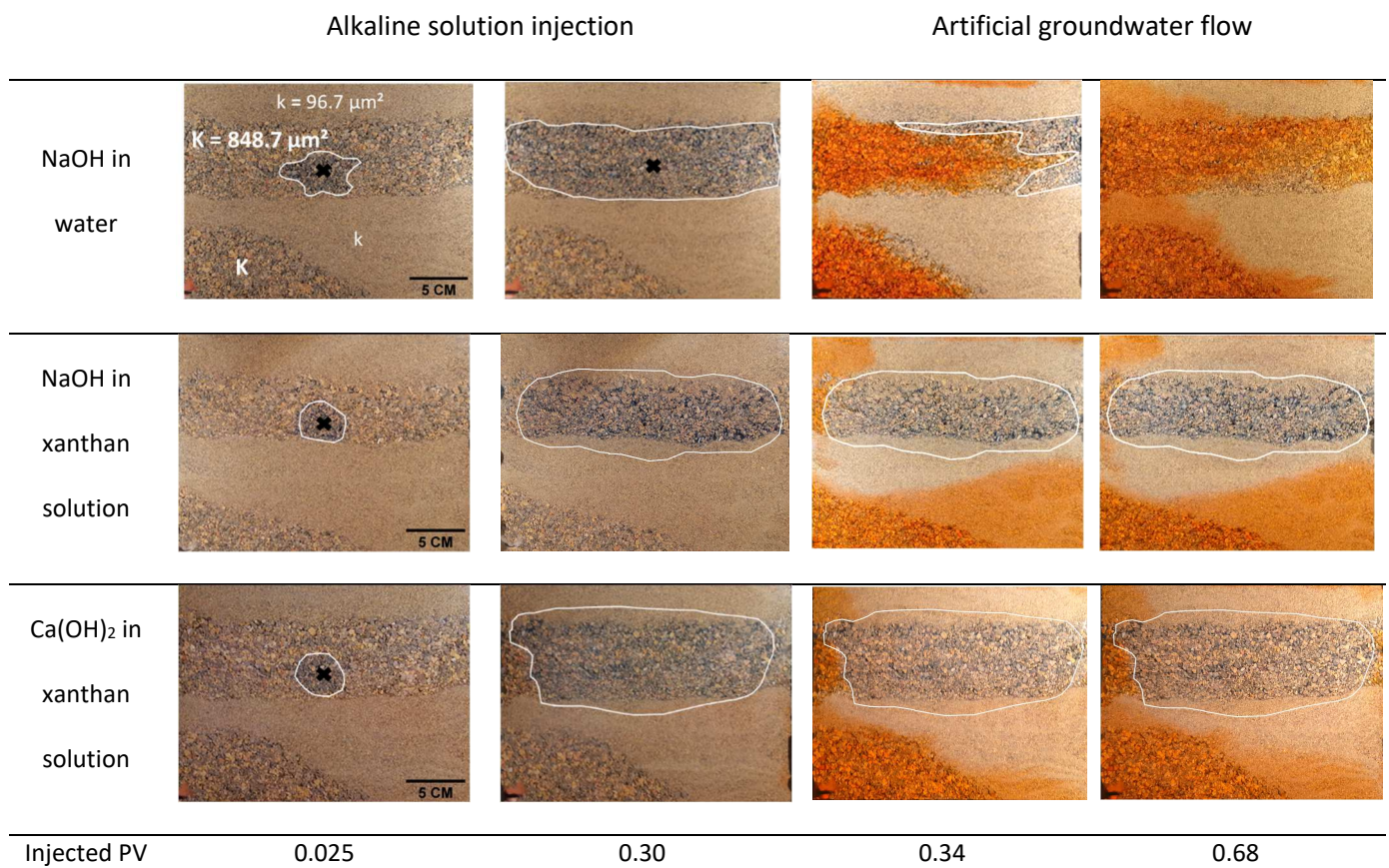
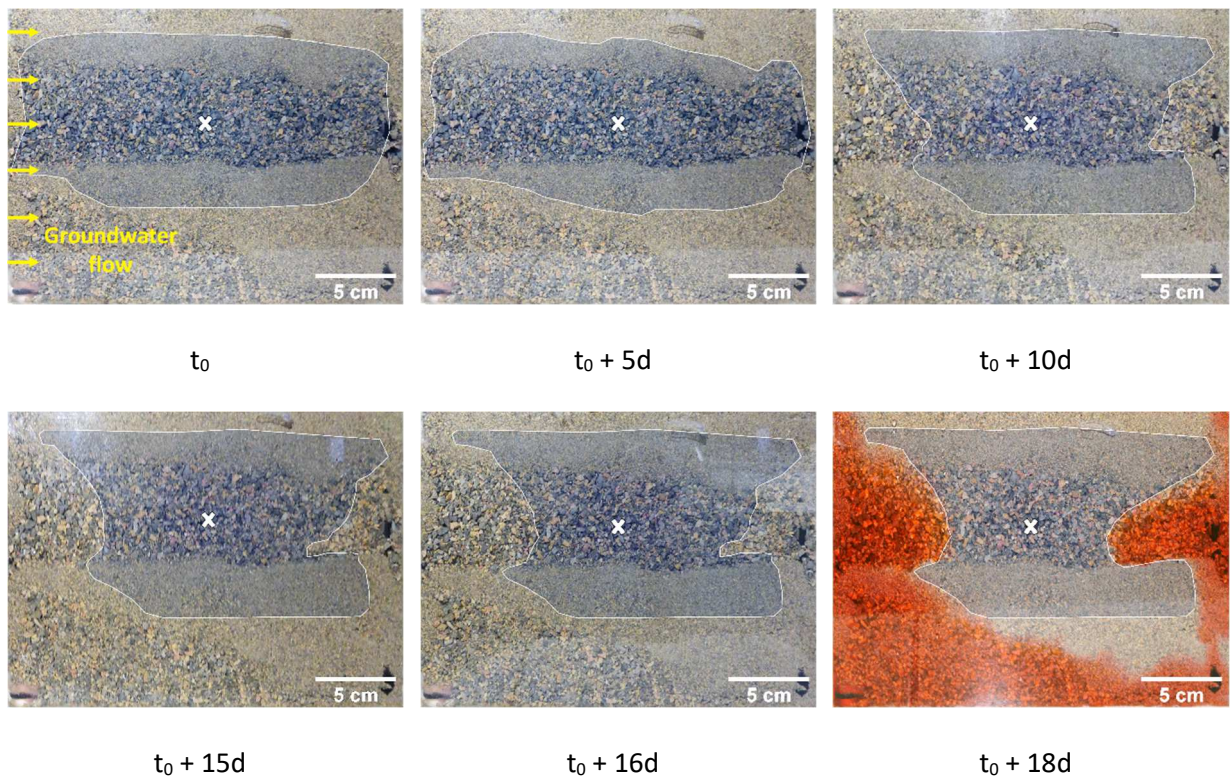


Figure 4. Comparison of alkalinity delivery and lateral sweeping after the delivery of alkalinity in permeability-

contrasted sandbox under water flow ( $10 \text{ m}\cdot\text{d}^{-1}$ ). The injection process is shown from left to right. The contacted area is delimited by the white solid line.

350

351 The persistence of the  $\text{Ca}(\text{OH})_2$  suspension in xanthan solution injected in the HPM was studied over  
352 18 d (Fig.5), which corresponds to more than 150 PV of GW. The model GW was colored after 18 d to  
353 allow a better visualization. Whereas no change could be detected in the treated zone filled with the  
354  $\text{Ca}(\text{OH})_2$  suspension in xanthan solution, the erosion of this viscous gel was observed after 9 d. The  
355 erosion mainly arose in the HPM, both up- and down-stream, with an average  $4.6 \times 10^{-3} \text{ m}\cdot\text{d}^{-1}$  velocity.  
356 After 18 d, the treated zone was eroded by 20%, however, it remained strongly alkaline despite the  
357 diffusion. Considering the overall permeability of the medium, it felt from 533 to  $69 \mu\text{m}^2$  after the  
358  $\text{Ca}(\text{OH})_2$  suspension in xanthan solution was injected. After 18 d, it increased only to  $127.3 \mu\text{m}^2$ .  
359 These encouraging results suggest that the injection of reactive suspensions and their long-lasting  
360 activity, in strongly permeability-contrasted and high velocity aquifer may be achieved.



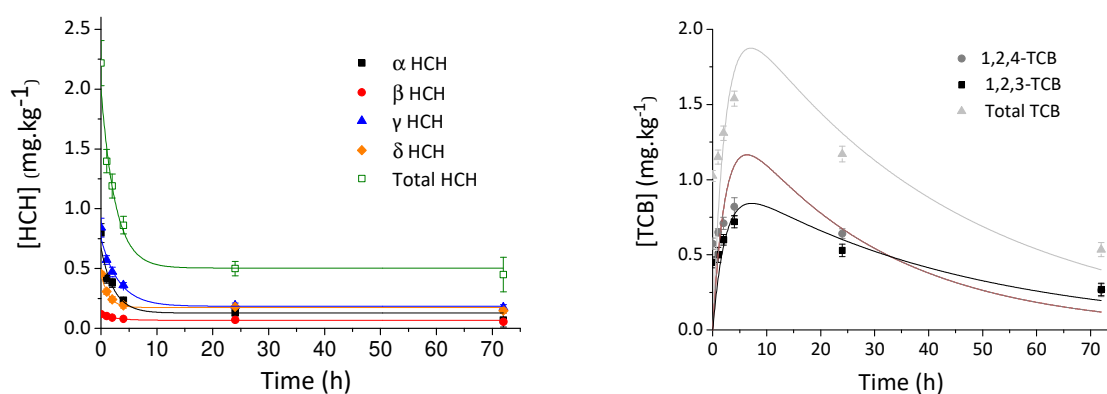


361 Figure 5. Photographs of lateral sweeping in permeability-contrasted sandbox under water flow (10  
362 m.d<sup>-1</sup>) after the delivery of a Ca(OH)<sub>2</sub> suspension in xanthan solution in the high permeability zone.

#### 363 4.2 Kinetics and mechanisms of contaminants degradation

364 The alkaline degradation of the HCHs and TCBs in the contaminated fine sand (9.9 μm<sup>2</sup>) was studied  
365 once the Ca(OH)<sub>2</sub> suspension in xanthan solution was injected. Degradation kinetics of these COCs  
366 present in the contaminated soil were pseudo-first order.

367



368

Figure 6. Alkaline degradation kinetics of HCHs (left) and time-dependance of TCBs concentrations (right) in the treated soils using the Ca(OH)<sub>2</sub> suspension in xanthan solution.

369 Kinetic documents shown in Fig. 6 indicate the fast degradation of HCHs at pH 12 and the production  
370 of 1,2,3-TCB and 1,2,4-TCB as metabolites, in agreement with the literature [73,74]. Two HCHs  
371 fractions were observed, a readily degradable one and an inert one. The most reactive fraction of  
372 HCHs was degraded within 17h regardless their initial concentrations, considering highest initial  
373 values of 4.2 mg.kg<sup>-1</sup>. This is consistent with reported values in aqueous solution for pHs close to 12  
374 [52,73]. As coarsely observed in our experiments, a linear-relationship was found between the  
375 logarithm of the rate constant of γ-HCH hydrolysis and the pH, in alkaline solutions [73]. Considering  
376 the kinetic documents shown in Fig. 6, the measured pseudo-first order rate-constants were  $0.32 \pm$

377 0.03,  $0.12 \pm 0.01$ ,  $0.22 \pm 0.02$  and  $0.25 \pm 0.03$  h<sup>-1</sup> for  $\alpha$ ,  $\beta$ ,  $\gamma$  and  $\delta$  isomers, respectively. The reactivity  
378 of the isomers ranks as  $\alpha$ -HCH >  $\delta$ -HCH >  $\gamma$ -HCH >  $\beta$ -HCH, in agreement with the sequence reported  
379 in an alkaline ethanol/water solution, whereas the expected order from steric considerations is  $\alpha$ -  
380 HCH >  $\gamma$ -HCH >  $\delta$ -HCH >  $\beta$ -HCH [10,52]. Furthermore, the inert fraction of HCHs was minor, but its  
381 amount depended strongly on both the isomers and their initial concentrations in soils. For example,  
382 for  $\gamma$ -HCH, it varied between 7 and 21%, depending on the initial concentrations, but it ranged  
383 between 0.2 and 0.3 mg.kg<sup>-1</sup>. Considering the document in Fig. 6 (left), it amounted to 8.8, 45.8, 20.8  
384 and 32.3 % for  $\alpha$ ,  $\beta$ ,  $\gamma$  and  $\delta$  isomers, respectively. This order matches quite well their sorption  
385 potential, which follows  $\gamma$ -HCH <  $\alpha$ -HCH <  $\beta$ -HCH <  $\delta$ -HCH [10,12].

386 Regarding the metabolites, 1,2,4-TCB was the major product (57%), followed by 1,2,3-TCB (30%), in  
387 agreement with other authors [73,75]. 1,3,5-TCB was detected, but its concentrations were below  
388 the QL. Our results suggest a dehydrohalogenation of HCHs to pentachlorocyclohexene (PCCH)  
389 followed by TCBs, as previously observed in similar conditions [73,75]. PCCH was identified as  
390 intermediate, based on the NIST-library, but not quantified in absence of standard. Yet,  
391 tetrachlorocyclohexadienes were not detected. Regarding the risks associated with the production of  
392 hazardous metabolites, phenols, hexachlorobenzene, pentachlorobenzene, tetrachlorobenzenes,  
393 dibenzodioxins (PCDDs) and polychlorinated dibenzofurans (PCDFs) were systematically sought, but  
394 never detected in these conditions. Yet, considering the degradation of concentrated HCHs mixtures  
395 in a methanol/water solution at pH 12, the sum of PCDFs amounted to 400 pg.L<sup>-1</sup>, which represented  
396 10<sup>-5</sup> % of the mass balance on the HCHs degradation.

397 After 24 and 72h of reaction, TCBs, DCBs, MCB and benzene were identified as metabolites.  
398 However, the last three compounds were below the QL. In contrast to what is reported in pure  
399 water, TCBs were not end products [73]. First order degradation rate-constants were  $0.023 \pm 0.017$   
400 and  $0.036 \pm 0.021$  h<sup>-1</sup> for 1,2,3-TCB and 1,2,4-TCB, respectively, and the calculated half-lives  
401 amounted to 25h. Even if the mechanism of TCBs degradation is unclear, deacetylation of xanthan

402 which takes place at  $\text{pH} > 9$ , may produce an e-donor compound, required for the reductive  
403 hydrogenolysis of the chlorobenzenes [76–78]. Furthermore, air-sparging is also effective to remove  
404 TCBs from the contaminated GW, given their Henry constants and vapor pressures [79].

405

## 406 5. Conclusion

407 Xanthan gels were assessed to perform the alkaline dechlorination of HCHs and their TCBs  
408 metabolites in a sedimentary aquifer of strong permeability contrast and high velocity. The alkaline  
409 degradation was selected because of the low cost of NaOH and  $\text{Ca}(\text{OH})_2$ . Despite the fact that strong  
410 alkalinity and  $\text{Ca}(\text{OH})_2$  microparticles have harmful effects on the viscosity of xanthan gels, this  
411 property is maintained, and so is their shear-thinning behavior. In contrast to water solution, the  
412 alkaline gels have shown a lack of fingering and an enhanced sweeping during their propagation  
413 through an anisotropic sandbox with a high permeability contrast. Considering the shear-thinning  
414 behavior of the xanthan gels, injections should be performed at a velocity that is as high as possible,  
415 while avoiding soil fracturing. Anticipated injection velocities in the field should range from 1.8 to 4  
416  $\text{m}\cdot\text{h}^{-1}$ , considering the range of soil permeability. Breakthrough curves for the alkaline xanthan  
417 solutions carried out in a silty sand demonstrated the fast and high transmission of the alkalinity at  
418 low pressure. Injected xanthan gels demonstrated a persistent blocking effect in the treated zone  
419 and GW flow diversion. Considering all the results, the use of NaOH in xanthan solution is  
420 recommended. Despite the high velocity GW flow, the long-lasting alkalinity in the treated zone  
421 matched the degradation of most of HCHs and their TCBs metabolites. Yet, the occurrence of CBs  
422 dichlorination in xanthan deserves further study. This shear-thinning gels technology is therefore  
423 promising for the ISR of anisotropic aquifers contaminated by slowly desorbing contaminants.

## 424 6. Acknowledgments

425 This research was carried out as a part of the FAMOUS project funded by the French Management  
426 Agency of Energy and Environment. The authors acknowledge Sarah Caradec for chemical analysis  
427 and Laura Fatin-Rouge for her help to improve the English of the manuscript.

428

## 429 7. References

430 [1] A. Chávez, C. Maya, R. Gibson, B. Jiménez, The removal of microorganisms and organic  
431 micropollutants from wastewater during infiltration to aquifers after irrigation of farmland in  
432 the Tula Valley, Mexico, *Environ. Pollut.* 159 (2011) 1354–1362.  
433 doi:10.1016/j.envpol.2011.01.008.

434 [2] M. Oteng-Peprah, M.A. Acheampong, N.K. deVries, Greywater Characteristics, Treatment  
435 Systems, Reuse Strategies and User Perception—a Review, *Water. Air. Soil Pollut.* 229 (2018).  
436 doi:10.1007/s11270-018-3909-8.

437 [3] *Commissariat général au développement durable, L'eau et les milieux aquatiques,*  
438 *CGDD/SOES. Paris, 2016.*

439 [4] V. Antoni, *Basol : un panorama des sites et sols pollués, ou potentiellement pollués,*  
440 *nécessitant une action des pouvoirs publics, Paris, 2013.*

441 [5] P. Bhatt, M.S. Kumar, T. Chakrabarti, Fate and degradation of POP-hexachlorocyclohexane,  
442 *Crit. Rev. Environ. Sci. Technol.* 39 (2009) 655–695. doi:10.1080/10643380701798306.

443 [6] J. Vijgen, P.C. Abhilash, Y.F. Li, R. Lal, M. Forter, J. Torres, N. Singh, M. Yunus, C. Tian, A.  
444 Schäffer, R. Weber, Hexachlorocyclohexane (HCH) as new Stockholm Convention POPs—a  
445 global perspective on the management of Lindane and its waste isomers, *Environ. Sci. Pollut.*  
446 *Res.* 18 (2011) 152–162. doi:10.1007/s11356-010-0417-9.

447 [7] J.A. Salam, N. Das, Remediation of lindane from environment - an overview, *Int. J. Adv. Biol.*  
448 *Res.* 2 (2012) 9–15. doi:10.1666/0094-8373(2001)027<0485:AOESGI>2.0.CO;2.



- 449 [8] R. Lal, G. Pandey, P. Sharma, K. Kumari, S. Malhotra, R. Pandey, V. Raina, H.-P.E. Kohler, C.  
450 Holliger, C. Jackson, J.G. Oakeshott, *Biochemistry of Microbial Degradation of*  
451 *Hexachlorocyclohexane and Prospects for Bioremediation*, *Microbiol. Mol. Biol. Rev.* 74 (2010)  
452 58–80. doi:10.1128/mnbr.00029-09.
- 453 [9] C.M. Dominguez, S. Rodriguez, D. Lorenzo, A. Romero, A. Santos, *Degradation of*  
454 *Hexachlorocyclohexanes (HCHs) by Stable Zero Valent Iron (ZVI) Microparticles*, *Water. Air.*  
455 *Soil Pollut.* 227 (2016). doi:10.1007/s11270-016-3149-8.
- 456 [10] S. Li, D.W. Elliott, S.T. Spear, L. Ma, W.X. Zhang, *Hexachlorocyclohexanes in the environment:*  
457 *Mechanisms of dechlorination*, *Crit. Rev. Environ. Sci. Technol.* 41 (2011) 1747–1792.  
458 doi:10.1080/10643389.2010.481592.
- 459 [11] C.M. Dominguez, A. Romero, A. Santos, *Selective removal of chlorinated organic compounds*  
460 *from lindane wastes by combination of nonionic surfactant soil flushing and Fenton oxidation*,  
461 *Chem. Eng. J.* (2018). doi:10.1016/j.cej.2018.09.170.
- 462 [12] S. Wacławek, D. Silvestri, P. Hrabák, V.V.T. Padil, R. Torres-Mendieta, M. Wacławek, M. Černík,  
463 D.D. Dionysiou, *Chemical oxidation and reduction of hexachlorocyclohexanes: A review*,  
464 *Water Res.* 162 (2019) 302–319. doi:10.1016/j.watres.2019.06.072.
- 465 [13] US EPA, *In Situ Treatment Technologies for Contaminated Soil*, 2006.
- 466 [14] A. Muggeridge, A. Cockin, K. Webb, H. Frampton, I. Collins, T. Moulds, P. Salino, *Recovery*  
467 *rates, enhanced oil recovery and technological limits*, *Philos. Trans. R. Soc. A Math. Phys. Eng.*  
468 *Sci.* 372 (2014). doi:10.1098/rsta.2012.0320.
- 469 [15] O. Atteia, E. Del Campo Estrada, H. Bertin, *Soil flushing: A review of the origin of efficiency*  
470 *variability*, *Rev. Environ. Sci. Biotechnol.* 12 (2013) 379–389. doi:10.1007/s11157-013-9316-0.
- 471 [16] K.R. Reddy, *Technical Challenges to In-situ Remediation of Polluted Sites*, *Geotech. Geol. Eng.*  
472 28 (2010) 211–221. doi:10.1007/s10706-008-9235-y.

- 473 [17] P. Ohrstrom, M. Persson, J. Albergel, P. Zante, S. Nasri, R. Berndtsson, J. Olsson, Field-scale  
474 variation of preferential flow as indicated from dye coverage, *J. Hydrol.* 257 (2002) 164–173.
- 475 [18] S.E. Allaire, S. Roulier, A.J. Cessna, Quantifying preferential flow in soils: A review of different  
476 techniques, *J. Hydrol.* 378 (2009) 179–204. doi:10.1016/j.jhydrol.2009.08.013.
- 477 [19] Y. Zhang, Z. Zhang, Z. Ma, J. Chen, J. Akbar, S. Zhang, C. Che, M. Zhang, A. Cerdà, A review of  
478 preferential water flow in soil science, *Can. J. Soil Sci.* 98 (2018) 604–618. doi:10.1139/cjss-  
479 2018-0046.
- 480 [20] I. Bouzid, J. Maire, S.I. Ahmed, N. Fatin-Rouge, Enhanced remedial reagents delivery in  
481 unsaturated anisotropic soils using surfactant foam, *Chemosphere.* 210 (2018).  
482 doi:10.1016/j.chemosphere.2018.07.081.
- 483 [21] I. Bouzid, J. Maire, N. Fatin-Rouge, Comparative assessment of a foam-based oxidative  
484 treatment of hydrocarbon-contaminated unsaturated and anisotropic soils, *Chemosphere.*  
485 233 (2019) 667–676. doi:10.1016/j.chemosphere.2019.05.295.
- 486 [22] X. Shen, L. Zhao, Y. Ding, B. Liu, H. Zeng, L. Zhong, X. Li, Foam, a promising vehicle to deliver  
487 nanoparticles for vadose zone remediation, *J. Hazard. Mater.* 186 (2011) 1773–1780.  
488 doi:10.1016/j.jhazmat.2010.12.071.
- 489 [23] I. Bouzid, D. Pino Herrera, M. Dierick, Y. Pechaud, V. Langlois, P.Y. Klein, J. Albaric, N. Fatin-  
490 Rouge, A new foam-based method for the (bio)degradation of hydrocarbons in contaminated  
491 vadose zone, *J. Hazard. Mater.* 401 (2021) 123420. doi:10.1016/j.jhazmat.2020.123420.
- 492 [24] D. O'Connor, D. Hou, Y.S. Ok, Y. Song, A.K. Sarmah, X. Li, F.M.G. Tack, Sustainable in situ  
493 remediation of recalcitrant organic pollutants in groundwater with controlled release  
494 materials: A review, *J. Control. Release.* 283 (2018) 200–213.  
495 doi:10.1016/j.jconrel.2018.06.007.
- 496 [25] R. Lenormand, E. Touboul, C. Zarcone, Numerical models and experiments on immiscible

- 497 displacements in porous media, *J. Fluid Mech.* 189 (1988) 165–187.  
498 doi:10.1017/S0022112088000953.
- 499 [26] L.W. Lake, *Enhanced oil recovery.*, Prentice Hall Englewood Cliffs, NJ, 1989.
- 500 [27] D.A.Z. Wever, F. Picchioni, A.. Broekhuis, *Polymers for enhanced oil recovery: A paradigm for*  
501 *structure–property relationship in aqueous solution*, *Prog. Polym. Sci.* 36 (2011) 1558–1628.
- 502 [28] X. Xu, A. Saeedi, K. Liu, *An experimental study of combined foam/surfactant polymer (sP)*  
503 *flooding for carbone dioxide-enhanced oil recovery (CO<sub>2</sub> -EOR)*, *J. Pet. Sci. Eng.* 149 (2017)  
504 603–611. doi:10.1016/j.petrol.2016.11.022.
- 505 [29] C. Wei, J. Zheng, L. Xiong, Z. Li, J. Yang, J. Zhang, S. Lin, L. Zhou, L. Fang, Y. Ding, *Evaluation and*  
506 *utilization of nano-micron polymer plug for heterogeneous carbonate reservoir with thief*  
507 *zones*, *Adv. Polym. Technol.* 2020 (2020). doi:10.1155/2020/3498583.
- 508 [30] K.S. Sorbie, R.S. Seright, *P. Recovery, Gel Placement in Heterogeneous Systems With*  
509 *Crossflow*, in: *SPE, Society of Petroleum Engineers, Tulsa, Oklahoma, 1992: p. 369.*  
510 doi:https://doi.org/10.2118/24192-MS.
- 511 [31] T. Tosco, F. Gastone, R. Sethi, *Guar gum solutions for improved delivery of iron particles in*  
512 *porous media (Part 2): Iron transport tests and modeling in radial geometry*, *J. Contam.*  
513 *Hydrol.* 166 (2014) 34–51. doi:10.1016/j.jconhyd.2014.06.014.
- 514 [32] L. Zhong, M. Oostrom, M.J. Truex, V.R. Vermeul, J.E. Szecsody, *Rheological behavior of*  
515 *xanthan gum solution related to shear thinning fluid delivery for subsurface remediation*, *J.*  
516 *Hazard. Mater.* 244–245 (2013) 160–170. doi:10.1016/j.jhazmat.2012.11.028.
- 517 [33] J. Xin, F. Tang, X. Zheng, H. Shao, O. Kolditz, *Transport and retention of xanthan gum-*  
518 *stabilized microscale zero-valent iron particles in saturated porous media*, *Water Res.* 88  
519 (2016) 199–206. doi:10.1016/j.watres.2015.10.005.

- 520 [34] J. Xin, J. Han, X. Zheng, H. Shao, O. Kolditz, Mechanism insights into enhanced  
521 trichloroethylene removal using xanthan gum-modified microscale zero-valent iron particles,  
522 *J. Environ. Manage.* 150 (2015) 420–426. doi:10.1016/j.jenvman.2014.12.022.
- 523 [35] S.C. Hauswirth, P.S. Birak, S.C. Rylander, C.T. Miller, Mobilization of manufactured gas plant  
524 tar with alkaline flushing solutions, *Environ. Sci. Technol.* 46 (2012) 426–433.  
525 doi:10.1021/es202278s.
- 526 [36] I. Bouzid, J. Maire, N. Fatin-rouge, Comparative assessment of a foam-based method for ISCO  
527 of coal tar contaminated unsaturated soils, *J. Environ. Chem. Eng.* 7 (2019) 103346.  
528 doi:10.1016/j.jece.2019.103346.
- 529 [37] J. Maire, A. Coyer, N. Fatin-rouge, Surfactant foam technology for in situ removal of heavy  
530 chlorinated, *J. Hazard. Mater.* 299 (2015) 630–638. doi:10.1016/j.jhazmat.2015.07.071.
- 531 [38] J. Maire, A. Joubert, D. Kaifas, T. Invernizzi, J. Marduel, S. Colombano, D. Cazaux, C. Marion, P.  
532 Klein, A. Dumestre, N. Fatin-rouge, Assessment of flushing methods for the removal of heavy  
533 chlorinated compounds DNAPL in an alluvial aquifer, *Sci. Total Environ.* 612 (2018) 1149–  
534 1158. doi:10.1016/j.scitotenv.2017.08.309.
- 535 [39] J. Maire, N. Fatin-Rouge, Surfactant foam flushing for in situ removal of DNAPLs in shallow  
536 soils, *J. Hazard. Mater.* 321 (2017) 247–255. doi:10.1016/j.jhazmat.2016.09.017.
- 537 [40] F. Gastone, T. Tosco, R. Sethi, Guar gum solutions for improved delivery of iron particles in  
538 porous media (Part 1): Porous medium rheology and guar gum-induced clogging, *J. Contam.*  
539 *Hydrol.* 166 (2014) 23–33. doi:10.1016/j.jconhyd.2014.06.013.
- 540 [41] S. Comba, D. Dalmazzo, E. Santagata, R. Sethi, Rheological characterization of xanthan  
541 suspensions of nanoscale iron for injection in porous media, *J. Hazard. Mater.* 185 (2011)  
542 598–605. doi:10.1016/j.jhazmat.2010.09.060.
- 543 [42] K.E. Martel, R. Martel, R. Lefebvre, P.J. Gélinas, Laboratory Study of Polymer Solutions Used

- 544 for Mobility Control During In Situ NAPL Recovery, *Groundw. Monit. Remediat.* (1998) 103–  
545 113. doi:<https://doi.org/10.1111/j.1745-6592.1998.tb00734.x>.
- 546 [43] M. Usman, O. Tascone, P. Faure, K. Hanna, Chemical oxidation of hexachlorocyclohexanes  
547 (HCHs) in contaminated soils, *Sci. Total Environ.* 476–477 (2014) 434–439.  
548 doi:10.1016/j.scitotenv.2014.01.027.
- 549 [44] R. García-Cervilla, A. Santos, A. Romero, D. Lorenzo, Remediation of soil contaminated by  
550 lindane wastes using alkaline activated persulfate: Kinetic model, *Chem. Eng. J.* 393 (2020)  
551 124646.
- 552 [45] C.M. Dominguez, A. Romero, D. Lorenzo, A. Santos, Thermally activated persulfate for the  
553 chemical oxidation of chlorinated organic compounds in groundwater, *J. Environ. Manage.*  
554 261 (2020) 110240. doi:10.1016/j.jenvman.2020.110240.
- 555 [46] B. Karn, T. Kuiken, M. Otto, Nanotechnology and in situ remediation: A review of the benefits  
556 and potential risks, *Environ. Health Perspect.* 117 (2009) 1823–1831.  
557 doi:10.1289/ehp.0900793.
- 558 [47] P. Oprčkal, A. Mladenovič, J. Vidmar, A. Mauko Pranjić, R. Milačić, J. Ščančar, Critical  
559 evaluation of the use of different nanoscale zero-valent iron particles for the treatment of  
560 effluent water from a small biological wastewater treatment plant, *Chem. Eng. J.* 321 (2017)  
561 20–30.
- 562 [48] H. Wang, S. Cai, L. Shan, M. Zhuang, N. Li, G. Quan, J. Yan, Adsorptive and reductive removal  
563 of chlorophenol from wastewater by biomass-derived mesoporous carbon-supported sulfide  
564 nanoscale zerovalent iron, *Nanomaterials.* 9 (2019) 1–12. doi:10.3390/nano9121786.
- 565 [49] D. Lorenzo, R. García-Cervilla, A. Romero, A. Santos, Partitioning of chlorinated organic  
566 compounds from dense non-aqueous phase liquids and contaminated soils from lindane  
567 production wastes to the aqueous phase, *Chemosphere.* 239 (2020) 124798.

- 568 doi:10.1016/j.chemosphere.2019.124798.
- 569 [50] P. Österreicher-Cunha, T. Langenbach, J.P.M. Torres, A.L.C. Lima, T.M.P. De Campos, E.D.A.  
570 Vargas, A.R. Wagener, HCH distribution and microbial parameters after liming of a heavily  
571 contaminated soil in Rio de Janeiro, *Environ. Res.* 93 (2003) 316–327. doi:10.1016/S0013-  
572 9351(03)00091-4.
- 573 [51] J.P.M. Torres, C.I.R. Fróes-Asmus, R. Weber, J.M.H. Vijgen, HCH contamination from former  
574 pesticide production in Brazil-a challenge for the Stockholm Convention implementation,  
575 *Environ. Sci. Pollut. Res.* 20 (2013) 1951–1957. doi:10.1007/s11356-012-1089-4.
- 576 [52] S. Cristol, The kinetics of the alkaline dehydrochlorination of the benzene hexachloride  
577 isomers. The mechanism of second-order elimination reactions., *J. Am. Chem. Soc.* 69 (1947)  
578 338–342.
- 579 [53] I. Watson, A. Burnett, *Hydrology: an Environmental Approach*, 1st Editio, CRC Press, 1995.  
580 doi:<https://doi.org/10.1201/9780203751442>.
- 581 [54] M. Fireman, Permeability Measurements On Disturbed Soil Samples, *Soil Sci.* 58 (1944) 337–  
582 354.
- 583 [55] M. Carter, E. Gregorich, *Soil sampling and methods of analysis*, 2nd editio, 2007.  
584 doi:<https://doi.org/10.1201/9781420005271>.
- 585 [56] A. Ogata, R.B. Banks, A solution of the differential equation of longitudinal dispersion in  
586 porous media, *Geol. Surv. (U.S.); Prof. Pap.* (1961) A1–A7.  
587 <http://pubs.er.usgs.gov/publication/pp411A>.
- 588 [57] M.M. Cross, Rheology of non-Newtonian fluids: A new flow equation for pseudoplastic  
589 systems, *J. Colloid Sci.* 20 (1965) 417–437. doi:10.1016/0095-8522(65)90022-X.
- 590 [58] G. Chauveteau, Rodlike Polymer Solution Flow through Fine Pores: Influence of Pore Size on

- 591 Rheological Behavior, *J. Rheol.* (N. Y. N. Y). 26 (1982) 111–142. doi:10.1122/1.549660.
- 592 [59] J.J. Sheng, Critical review of alkaline-polymer flooding, *J. Pet. Explor. Prod. Technol.* 7 (2017)  
593 147–153. doi:10.1007/s13202-016-0239-5.
- 594 [60] T. Tosco, R. Sethi, Transport of non-newtonian suspensions of highly concentrated micro- and  
595 nanoscale iron particles in porous media: A modeling approach, *Environ. Sci. Technol.* 44  
596 (2010) 9062–9068. doi:10.1021/es100868n.
- 597 [61] L. Ren, J. Dong, Z. Chi, Y. Li, Y. Zhao, E. Jianan, Rheology modification of reduced graphene  
598 oxide based nanoscale zero valent iron (nZVI/rGO) using xanthan gum (XG): Stability and  
599 transport in saturated porous media, *Colloids Surfaces A Physicochem. Eng. Asp.* 562 (2019)  
600 34–41. doi:10.1016/j.colsurfa.2018.11.013.
- 601 [62] L. Zhong, M. Oostrom, T.W. Wietsma, M.A. Covert, Enhanced remedial amendment delivery  
602 through fluid viscosity modifications: Experiments and numerical simulations, *J. Contam.*  
603 *Hydrol.* 101 (2008) 29–41. doi:10.1016/j.jconhyd.2008.07.007.
- 604 [63] US EPA, Hydraulic fracturing technology, EPA 540-R-93-505. (1993) 140.
- 605 [64] J. Maire, E. Brunol, N. Fatin-Rouge, Shear-thinning fluids for gravity and anisotropy mitigation  
606 during soil remediation in the vadose zone, *Chemosphere.* 197 (2018) 661–669.  
607 doi:10.1016/j.chemosphere.2018.01.101.
- 608 [65] E. Dalla Vecchia, M. Luna, R. Sethi, Transport in porous media of highly concentrated iron  
609 micro- and nanoparticles in the presence of xanthan gum, *Environ. Sci. Technol.* 43 (2009)  
610 8942–8947. doi:10.1021/es901897d.
- 611 [66] A. Tiraferri, R. Sethi, Enhanced transport of zerovalent iron nanoparticles in saturated porous  
612 media by guar gum, *J. Nanoparticle Res.* 11 (2009) 635–645. doi:10.1007/s11051-008-9405-0.
- 613 [67] B. Liang, Y. Xie, Z. Fang, E.P. Tsang, Assessment of the transport of polyvinylpyrrolidone-

- 614 stabilised zero-valent iron nanoparticles in a silica sand medium, *J. Nanoparticle Res.* 16  
615 (2014). doi:10.1007/s11051-014-2485-0.
- 616 [68] L. Shi, J. Chen, Q. Wang, X. Song, Effects of carrier on the transport and DDT removal  
617 performance of nano-zerovalent iron in packed sands, *Chemosphere*. 209 (2018) 489–495.  
618 doi:10.1016/j.chemosphere.2018.06.123.
- 619 [69] Y. Ding, B. Liu, X. Shen, L. Zhong, X. Li, Foam-Assisted Delivery of Nanoscale Zero Valent Iron in  
620 Porous Media, *J. Environ. Eng.* 139 (2013) 1206–1212. doi:10.1061/(ASCE)EE.1943-  
621 7870.0000727.
- 622 [70] Y. Liang, S.A. Bradford, J. Simunek, M. Heggen, H. Vereecken, E. Klumpp, Retention and  
623 remobilization of stabilized silver nanoparticles in an undisturbed loamy sand soil, *Environ.*  
624 *Sci. Technol.* 47 (2013) 12229–12237. doi:10.1021/es402046u.
- 625 [71] T. Robert, R. Martel, S.H. Conrad, R. Lefebvre, U. Gabriel, Visualization of TCE recovery  
626 mechanisms using surfactant-polymer solutions in a two-dimensional heterogeneous sand  
627 model, *J. Contam. Hydrol.* 86 (2006) 3–31. doi:10.1016/j.jconhyd.2006.02.013.
- 628 [72] A. Tran-Viet, A. F. Routh, A. W. Woods, Control of the Permeability of a Porous Media Using a  
629 Thermally Sensitive Polymer, *AIChE J.* 60 (2014). doi:10.1002/aic.14352.
- 630 [73] X. Liu, P. Peng, J. Fu, W. Huang, Effects of FeS on the transformation kinetics of lindane,  
631 *Environ. Sci. Technol.* 43 (2003) 1062–1067.
- 632 [74] A. Santos, J. Fernandez, S. Rodriguez, C.M. Dominguez, M.A. Lominchar, D. Lorenzo, A.  
633 Romero, Abatement of chlorinated compounds in groundwater contaminated by HCH wastes  
634 using ISCO with alkali activated persulfate, *Sci. Total Environ.* 615 (2018) 1070–1077.  
635 doi:10.1016/j.scitotenv.2017.09.224.
- 636 [75] A. Santos, J. Fernández, J. Guadaño, D. Lorenzo, A. Romero, Chlorinated organic compounds in  
637 liquid wastes (DNAPL) from lindane production dumped in landfills in Sabiñanigo (Spain),



638 Environ. Pollut. 242 (2018) 1616–1624. doi:10.1016/j.envpol.2018.07.117.

639 [76] E.P. Pinto, L. Furlan, C.T. Vendruscolo, Chemical deacetylation natural xanthan  
640 (Jungbunzlauer®), Polimeros. 21 (2011) 47–52. doi:10.1590/S0104-14282011005000005.




641 [77] J. He, Y. Sung, M.E. Dollhopf, B.Z. Fathepure, J.M. Tiedje, F.E. Löffler, Acetate versus hydrogen  
642 as direct electron donors to stimulate the microbial reductive dechlorination process at  
643 chloroethene-contaminated sites, Environ. Sci. Technol. 36 (2002) 3945–3952.  
644 doi:10.1021/es025528d.

645 [78] F. BRAHUSHI, F.O. KENGARA, Y. SONG, X. JIANG, J.C. MUNCH, F. WANG, Fate Processes of  
646 Chlorobenzenes in Soil and Potential Remediation Strategies: A Review, Pedosphere. 27  
647 (2017) 407–420. doi:10.1016/S1002-0160(17)60338-2.

648 [79] Agency for Toxic Substances and Disease Registry, Trichlorobenzenes, (2019).  
649 <https://www.atsdr.cdc.gov/ToxProfiles/tp.asp?id=1168&tid=255#bookmark08> (accessed June  
650 25, 2020).

651

652

-  Contaminated zone
-  Alkaline polymer solution
-  Groundwater flow

